The emergence of sarcomeric, graded-polarity and spindle-like patterns in bundles of short cytoskeletal polymers and two opposite molecular motors

2011 J. Phys.: Condens. Matter 23 374102

(http://iopscience.iop.org/0953-8984/23/37/374102)

IOP Publishing Journal of Physics: Condensed Matter

J. Phys.: Condens. Matter **23** (2011) 374102 (10pp) doi:10.1088/0953-8984/23/37/374102

The emergence of sarcomeric, graded-polarity and spindle-like patterns in bundles of short cytoskeletal polymers and two opposite molecular motors

E M Craig, S Dey and A Mogilner

Department of Neurobiology, Physiology and Behavior and Department of Mathematics, University of California, Davis, CA 95616, USA

E-mail: ecraig@ucdavis.edu, satarupa.dey@gmail.com and mogilner@math.ucdavis.edu

Received 19 January 2011, in final form 23 February 2011
Published 23 August 2011
Online at stacks.iop.org/JPhysCM/23/374102

Abstract

We use linear stability analysis and numerical solutions of partial differential equations to investigate pattern formation in the one-dimensional system of short dynamic polymers and one (plus-end directed) or two (one is plus-end, another minus-end directed) molecular motors. If polymer sliding and motor gliding rates are slow and/or the polymer turnover rate is fast, then the polymer–motor bundle has mixed polarity and homogeneous motor distribution. However, if motor gliding is fast, a sarcomeric pattern with periodic bands of alternating polymer polarity separated by motor aggregates evolves. On the other hand, if polymer sliding is fast, a graded-polarity bundle with motors at the center emerges. In the presence of the second, minus-end directed motor, the sarcomeric pattern is more ubiquitous, while the graded-polarity pattern is destabilized. However, if the minus-end motor is weaker than the plus-end directed one, and/or polymer nucleation is autocatalytic, and/or long polymers are present in the bundle, then a spindle-like architecture with a sorted-out polarity emerges with the plus-end motors at the center and minus-end motors at the edges. We discuss modeling implications for actin–myosin fibers and *in vitro* and meiotic spindles.

1. Introduction

Cell shape, motility, division and other behaviors depend on the cytoskeleton—a dynamic scaffold built from actin, microtubules and intermediate filaments together with molecular motors, binding proteins and other accessory molecules [1]. Actin filaments and microtubules are polar polymers characterized by distinct plus and minus-ends (barbed and pointed ends, respectively, in the case of actin; here we will call those plus- and minus-ends for simplicity). These polymers are very dynamic, often turning over in mere seconds, and are engaged in diverse processes of treadmilling, dynamic instability, severing and annealing [2]. Molecular motors are vast families of molecules in the cell that transduce chemical energy into mechanical force and movement and are crucial in cross-linking neighboring filaments and sliding them with respect to each other [3]. Dynamic systems of polymers and molecular motors that transport these polymers in the cell tend to self-organize [4]. This self-organization, which is of fundamental interest to both cell biology and biomedical applications [1], is the focus of our theoretical study.

We examine the dynamics of one-dimensional (1D) cytoskeletal bundles, which are amenable to simple mathematical modeling. Most notable examples of such actin bundles are muscle sarcomeres, and the stress fibers of an adherent cell [5, 6] in which actin filaments are arranged periodically in unipolar parallel bands interspersed with clusters of myosin II (just called myosin below) motors (figure 1(a)). In these stress fibers, tens of motor heads from each cluster reach to neighboring filaments and execute short power-strokes that tend to move myosin toward the filaments' plus-ends, and in return to slide the filaments in the direction of their minus-ends. This motor action leads to the opposite sliding of anti-parallel filament pairs (figure 1) and overall stress fiber contraction. Another ubiquitous and dynamic actin–myosin bundle is the contractile ring of dividing cells [7]. Less organized actin–

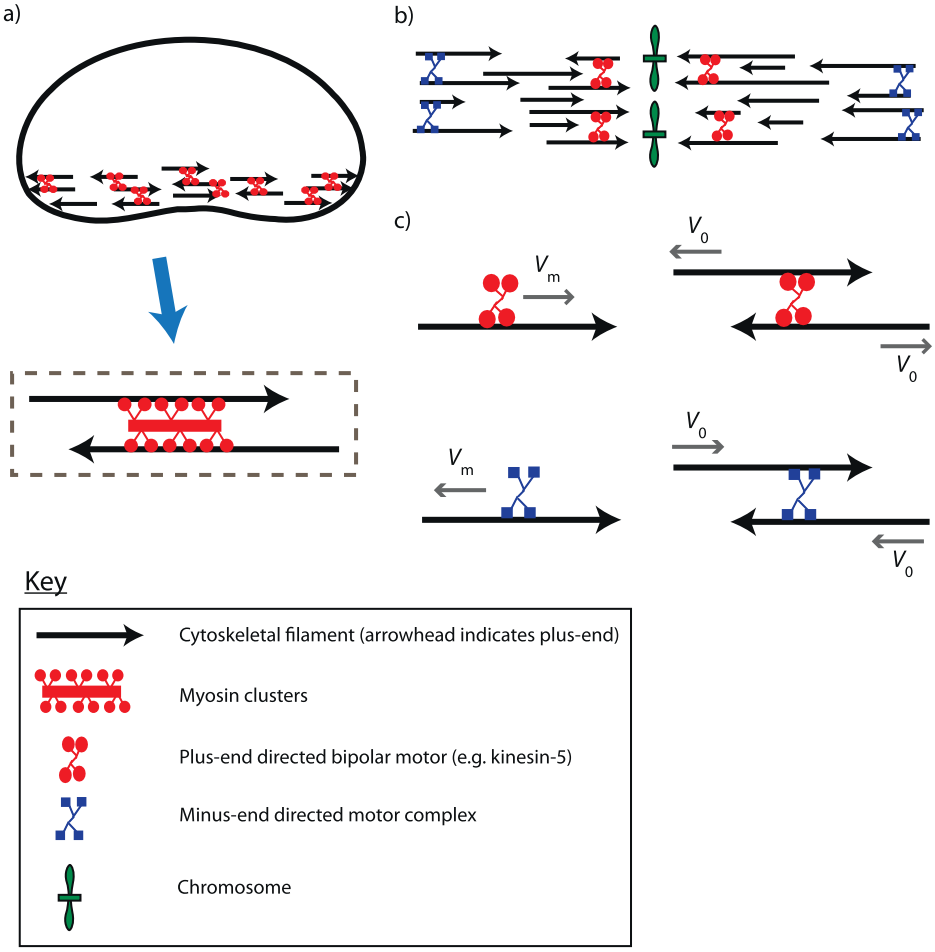

Figure 1. Schematic of polymer–motor bundles in the cell. (a) Actin–myosin bundles at the rear of a migrating cell. (b) Microtubule–motor organization in meiotic and *in vitro* spindles. (c) Illustration of motor and filament velocities introduced in section 2.
(This figure is in colour only in the electronic version)

myosin bundles are also observed in motile appendages of migrating cells [8]. In all these bundles, the actin filaments are much shorter than the whole bundle's length. An important open question is: are the spatial organizations of the actin–myosin bundles imposed by the cell [9] or self-organized?

Mitotic and meiotic spindles present examples of dynamic microtubule–motor bundles [10]. Microtubules of opposite polarity overlap at the spindle 'equator' where they interact with kinesin-5 motors (figure 1(b)). These motors are bipolar, having motor domains on both ends, which allow them to symmetrically slide apart anti-parallel microtubules [11]. This sliding of anti-parallel microtubules elongates the spindle [12] and is an important part of spindle maintenance. In mammalian spindles, most microtubules extend the half-length between the pole and the equator [13], but in meiotic and *in vitro* spindles that assemble in Xenopus egg extracts [14], the individual microtubules are much shorter. These spindles consist of many short microtubules crosslinked by motors [15]. In addition to kinesin-5 motors, these spindles contain cytoplasmic dynein motors that are, unlike kinesin-5, minus-end directed and not bipolar. Dyneins are proposed to bind one microtubule and transport it along another one toward a spindle pole, as well as to crosslink microtubules that are closer to the poles [16]. Importantly, the characteristic spindle-like pattern, in which kinesin-5 is at the equator and dynein is at the poles, and microtubules are oriented with their minus-ends toward the poles and plus-ends toward the equator (figure 1(b)), can self-assemble without centrosomes and chromosomes [17]. Both kinesin-5 and dynein motors are crucial for this self-organization [17–19], while other motor families active in the spindle are likely dispensable [3].

Here, we consider theoretically a simplistic case of polymer–motor self-organization inspired by actin–myosin bundle organization in motile cells and microtubule–kinesin–dynein organization in spindles. Theory of these systems attracted so much attention in the recent decade that we cannot cite all relevant papers. Largely speaking, three approaches were used in modeling the polymer–motor dynamics. A majority of studies used hydrodynamic-like equations for non-equilibrium biological gels based on symmetries and conservation laws of the system [20, 21]. More detailed models used integro-differential equations taking into account finite polymer length [22]. Yet other works employed discrete and stochastic agent-based computer simulations, in which the trajectory of each individual polymer was simulated [23–25]. Most of these studies were applied to microtubule–kinesin

systems, but actin–myosin patterns were also modeled [26]. Here, we continue the investigation started by all these studies, taking a general approach to the problem of pattern formation in filament bundles by considering continuous one-dimensional distributions of short polarized filaments and motors. We demonstrate that a great variety of observed patterns can be captured by solving very simple partial differential equations describing densities of polymers and motors and derived from using force balances and conservation laws. Interestingly, we find that periodic sarcomeric patterns are ubiquitous and stable, and that kinesin-5-like motors alone can organize the spindle-like pattern only if the microtubules slide very quickly. The sarcomeric pattern is stabilized further by the addition of a second, dynein-like motor, and a spindle-like pattern can form only if the dynein-like motor is much weaker than the kinesin motor. The model also clarifies how polymer stability, length and autocatalytic nucleation affect pattern formation.

2. Force balances and transport rates for motors and polymers

In the model, we derive the rates of the motor gliding and polymer sliding from the following force balances: in the case of the myosin cluster, a single motor head can be described by the force–velocity relation. Most frequently, a linear relation is used for simplicity [23, 25]:

$$f_{\mathrm{r,l}} = f_{\mathrm{m}}\left(1 \mp \frac{V_{\mathrm{mot}} - V_{\mathrm{r,l}}}{V_{\mathrm{m}}}\right), \tag{1}$$

where indices r, l stand for motor heads pulling on the right/left oriented polymers (with plus-ends directed to the right/left, respectively), f_{m} is the maximal (stall) force developed by the motor, V_{m} is the free gliding motor speed, V_{mot} is the velocity of the myosin cluster and $V_{\mathrm{r,l}}$ are the velocities of the right/left oriented polymers (figure 1(c)). We assume, also following majority of the published models, that the polymer velocities are proportional to the applied force:

$$V_{\mathrm{r,l}} = \mp f_{\mathrm{r,l}}/\zeta, \tag{2}$$

where ζ is the effective protein friction coefficient originating from transient attachments of the bundle polymer to the rest of the cytoskeleton [27]. The total force on a myosin cluster has to be equal to zero; assuming that the number of right/left oriented polymers interacting with the myosin cluster are proportional to the local densities of such polymers, P_{r}, P_{l}, we have:

$$P_{\mathrm{l}} f_{\mathrm{l}} = P_{\mathrm{r}} f_{\mathrm{r}}. \tag{3}$$

Five linear algebraic equations (1)–(3) with five unknowns (two forces and three velocities; equations (1) and (2) stand for two equations each) give the following expressions for the velocities of the motor clusters and two types of polymers (right/left oriented): $V_{\mathrm{mot}} = V_{\mathrm{m}}\frac{P_{\mathrm{r}}-P_{\mathrm{l}}}{P_{\mathrm{r}}+P_{\mathrm{l}}}$, $V_{\mathrm{r,l}} = \mp\frac{f_{\mathrm{m}}}{\zeta}\frac{P_{\mathrm{l,r}}}{P_{\mathrm{r}}+P_{\mathrm{l}}}$. We will call the variable $P = \frac{P_{\mathrm{r}}-P_{\mathrm{l}}}{P_{\mathrm{r}}+P_{\mathrm{l}}}$ the polarity. The analysis above was for one myosin cluster; introducing the myosin density, M, and parameter V_0, for the sliding speed of one polymer interacting with a unit myosin density in the presence of many oppositely oriented polymers, we have:

$$V_{\mathrm{mot}} = V_{\mathrm{m}} P, \qquad P = \frac{P_{\mathrm{r}} - P_{\mathrm{l}}}{P_{\mathrm{r}} + P_{\mathrm{l}}}, \qquad V_{\mathrm{r}} = -\frac{V_0 P_{\mathrm{l}} M}{P_{\mathrm{r}} + P_{\mathrm{l}}},$$
$$V_{\mathrm{l}} = \frac{V_0 P_{\mathrm{r}} M}{P_{\mathrm{r}} + P_{\mathrm{l}}}. \tag{4}$$

These formulas have a very simple meaning: in a region of uniform polarity, the motors have no net drift; in regions where the filaments are all co-aligned, the motors move with their free gliding speed toward the plus-ends; and in the general case of mixed filament polarity, this speed is factored by the local polarity, which is the normalized local difference between the right and left oriented polymers. The polymers drift in their minus-end direction with a velocity proportional to the local motor concentration and to the normalized local density of the opposite polarity polymers.

Although formulas (4) were derived with actin–myosin bundles in mind, they are more general than their model-specific derivation above implies. For example, the same formulas can be used to describe meiotic and *in vitro* spindles in which bipolar motors (e.g., kinesin-5) interact with short microtubules: if the motor density is small, then the interactions between polymers in the bundle are effectively pair-wise. This means that the motors connecting parallel polymers move toward the plus-ends with the free motor gliding speed, while the motors between an anti-parallel polymer pair do not move but instead slide the pair apart. Averaging over random pair-wise interactions, it is easy to see that for a right/left oriented polymer, the normalized number of interactions shifting it in its minus-end direction is $P_{\mathrm{l,r}}/(P_{\mathrm{r}} + P_{\mathrm{l}})$, respectively, leading to formulas (4) for $V_{\mathrm{r,l}}$. Similar averaging of the number of parallel polymer pairs shows that the average motor drift is proportional to the ratio $(P_{\mathrm{r}}^2 - P_{\mathrm{l}}^2)/(P_{\mathrm{r}} + P_{\mathrm{l}})^2 = (P_{\mathrm{r}} - P_{\mathrm{l}})/(P_{\mathrm{r}} + P_{\mathrm{l}}) = P$, again leading to formula (4) for V_{mot}. Finally, in the case of unipolar single motors of the dynein type, agent-based simulations result in average drifts similar to formulas (4) [25].

3. Reaction–drift–diffusion dynamics of the 1D polymer–motor bundle

For a system with a single type of plus-end directed motor (1-motor system), the conservation laws for two polymer densities and motor density have the form of the following reaction–drift–diffusion equations:

$$\partial_T P_{\mathrm{r,l}} = D_{\mathrm{p}}\partial_X^2 P_{\mathrm{r,l}} - \partial_X\left(V_{\mathrm{r,l}} P_{\mathrm{r,l}}\right) - \gamma P_{\mathrm{r,l}} + S,$$
$$\partial_T M = D_{\mathrm{m}}\partial_X^2 M - \partial_X\left(V_{\mathrm{mot}} M\right) + K_{\mathrm{on}} - K_{\mathrm{off}} M. \tag{5}$$

The drift terms are discussed in section 2. S is the constant rate of random polymer nucleation; γ is the rate of the polymer disassembly (turnover); K_{on} is the rate of motor attachment to the polymer, and K_{off} is the rate of motor detachment. Diffusion terms in the equations do not describe actual thermal diffusion, which is slow. Rather, in the case of microtubules, dynamic instability behavior can

under a number of conditions be considered an effective diffusion of the plus-end and center-of-mass coordinates of a polymer [28]. Similarly, processes of severing and annealing of actin filaments lead to random shifts of the polymers' centers of mass and, effectively, diffusion [29, 30]. Finally, the motors, in addition to a small diffusion when moving along single polymers [27], undergo effective diffusion because their drift rates fluctuate due to random interactions with pairs of polymers of different polarities. While these equations describe the 1-motor system, we will also later extend them to include two oppositely directed types of motors (2-motor system).

The natural scales in this system are the inverted polymer disassembly rate, γ^{-1}, for time, the ratio of the on- and off-rates, $K_{\rm on}/K_{\rm off}$, for the average motor density, the nucleation rate divided by the disassembly rate, S/γ, for the polymer densities, and the average polymer speed multiplied by the characteristic time, $V_{\rm p}/\gamma$, for distance. Introducing the non-dimensional variables, $t = \gamma T$, $m = K_{\rm off}M/K_{\rm on}$, $p_{\rm r,l} = P_{\rm r,l}\gamma/S$ and $x = \gamma X/V_{\rm p}$, we obtain the non-dimensionalized equations:

$$\begin{aligned} \partial_t p_{\rm r,l} &= \omega D\partial_x^2 p_{\rm r,l} \pm \beta\partial_x\left(\frac{p_{\rm r}p_{\rm l}m}{p_{\rm r}+p_{\rm l}}\right) - p_{\rm r,l} + 1, \\ \partial_t m &= D\partial_x^2 m - \partial_x\left(\frac{p_{\rm r}-p_{\rm l}}{p_{\rm r}+p_{\rm l}}m\right) + a\,(1-m)\,. \end{aligned} \tag{6}$$

The system behavior is determined by four non-dimensional parameter combinations:

$$\omega = \frac{D_{\rm p}}{D_{\rm m}}, \qquad D = \frac{D_{\rm m}\gamma}{V_{\rm m}^2}, \qquad \beta = \frac{V_0}{V_{\rm m}}\frac{K_{\rm on}}{K_{\rm off}}, \qquad a = \frac{K_{\rm off}}{\gamma}. \tag{7}$$

Introducing the characteristic filament sliding speed, $\tilde{V}_0 = V_0 K_{\rm on}/K_{\rm off}$, we can re-write parameter β as $\beta = \tilde{V}_0/V_{\rm m}$.

Note that our model has the following interesting features: adding the equations for the oppositely oriented filaments ($z = p_{\rm r} + p_{\rm l}$), we obtain the equation

$$\partial_t z = \omega D\partial_x^2 z - z + 2,$$

which shows that the net polymer density simply equilibrates to a constant $z = 2$, so there is neither contraction nor expansion of the polymer bundle, and the net polymer flux is zero. Substituting $p_{\rm r} + p_{\rm l} = 2$ into the difference between the equations for the oppositely oriented filaments, we obtain the following equations for the polarity ($p = (p_{\rm r} - p_{\rm l})/(p_{\rm r} + p_{\rm l})$) and motor densities: $\partial_t p = \omega D\partial_x^2 p - \beta\partial_x(mp^2) + \beta\partial_x m - p$, $\partial_t m = D\partial_x^2 m - \partial_x(pm) + a(1-m)$.

One can see from the equation for the polarity that the spatial motor density gradients are a source/sink for the polarity, which means that local motor aggregates create jumps of polarity—effective local orientation of the polymers into the motor aggregate. The polarity also propagates with a drift rate proportional to the polarity itself, which reinforces the polarity jumps. The motors, on the other hand, drift in the direction of local polarity. Thus, we expect that if the effective diffusion and polymer disassembly are slow, then instabilities and spatial patterns should evolve in this system. The linear stability analysis and numerical solutions reported below confirm this intuition.

4. Characteristic parameters of the system

Characteristic parameters for the system can be estimated from the experimental literature. The characteristic size of short microtubules in *in vitro* spindles is in the 1 μm range [31]. Actin filaments in actin–myosin bundles have similar characteristic sizes [8, 32]. Both actin–myosin bundle length [8, 33] and spindle size [14, 34] are on the order of 10 μm. The characteristic gliding speed of molecular motors in the spindle is $V_{\rm m} \sim 0.2\ \mu{\rm m\,s^{-1}}$ [35]. Similar speeds are reported for myosin clusters in rapidly motile cells [36]. The characteristic sliding speed of actin filaments in rapidly motile cells could be as fast as $\tilde{V}_0 \sim 0.2\ \mu{\rm m\,s^{-1}}$ [36]. The microtubule sliding (called poleward flux in mitosis literature) is slow in both the *in vitro* and some *in vivo* spindles, on the order of $\tilde{V}_0 \sim 0.03$–$0.05\ \mu{\rm m\,s^{-1}}$ [37, 38]. The short MTs both in *in vitro* and some *in vivo* spindles are very dynamic, turning over in just a few seconds, such that $\gamma \sim 0.1\ {\rm s^{-1}}$ [31, 34]. Actin in the actin–myosin bundles in the rapidly motile cells disassembles with similar rates [8]. Detachment of the kinesin-5 motors from the microtubules in the spindles is quick, $K_{\rm off} \sim 0.5\ {\rm s^{-1}}$ [35]. Even faster, but similar rates are reported for dynein [39]. Myosin clusters that have tens of motor heads extending from each of them probably detach more slowly; no numbers are reported in the literature.

An effective diffusion coefficient for microtubules undergoing dynamic instability [28] can be estimated by dividing the square of the characteristic microtubule length, $L \sim 1\ \mu$m, by the average time, $\gamma^{-1} \sim 10$ s, of its complete disassembly: $D_{\rm p} \sim L^2/2\gamma^{-1} \sim 0.05\ \mu{\rm m^2\,s^{-1}}$. Interestingly, severing and annealing of actin filaments are characterized by the same effective diffusion coefficient [29, 30]. For example, the effective diffusion coefficient due to the severing process can be estimated by multiplying the square of the characteristic filament length, $L \sim 1\ \mu$m, by the average severing rate, $r \sim 0.1\ {\rm s^{-1}}$: $D_{\rm p} \sim L^2 r/2 \sim 0.05\ \mu{\rm m^2\,s^{-1}}$. Similarly, the effective diffusion coefficient of the motors can be estimated by multiplying the square of the average motor speed, $V_{\rm m} \sim 0.2\ \mu{\rm m\,s^{-1}}$, by the average time a motor stays attached, $1/K_{\rm off} \sim 2$ s,: $D_{\rm m} \sim V_{\rm m}^2/2K_{\rm off} \sim 0.05\ \mu{\rm m^2\,s^{-1}}$.

Using these parameters, we estimate the characteristic non-dimensional parameter combinations that determine the system behavior: for both actin–myosin bundles, and for the spindle, $D \sim 0.1$ and $\beta \sim 1$. For the spindle, where the motor's kinetics are fast compared to polymer turnover, we estimate $a \sim 5$. Actin–myosin bundles may have slower motor turnover as discussed above, corresponding to a smaller value of a. Finally, effective diffusion of polymers and motors is of the same order of magnitude, and simulations show that modest varying of the diffusion coefficients does not affect the results qualitatively, so in the analysis we kept the parameter $\omega = 1$ for simplicity. Thus, the effective diffusion of polymers and

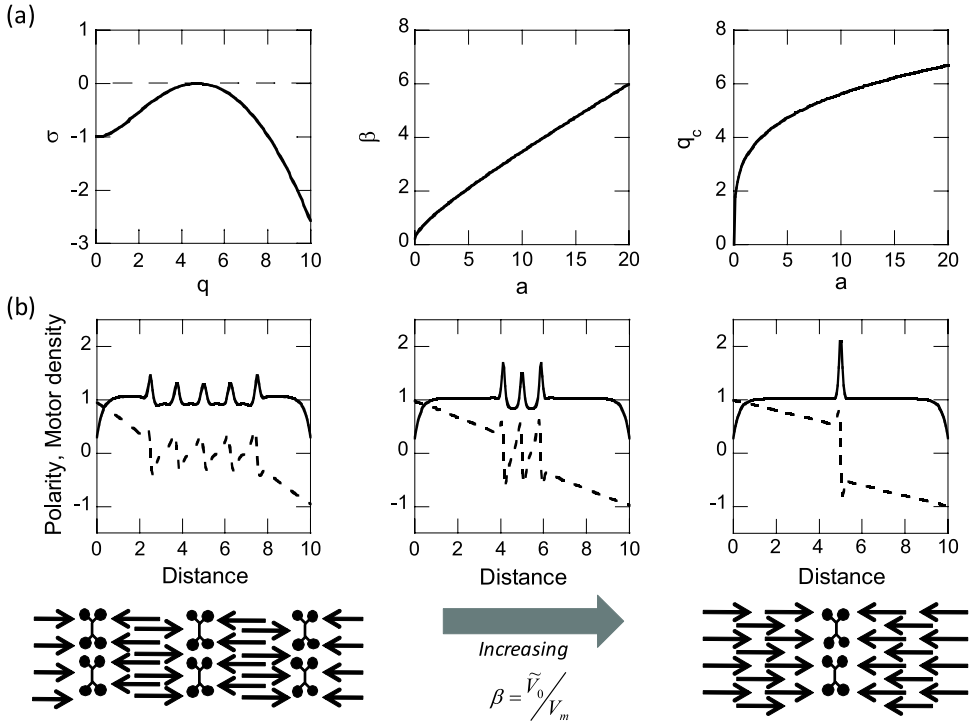

Figure 2. Results for polymer–motor bundles in the 1-motor system. (a) Linear stability analysis results (shown here for $D = 0.1$). Left: dispersion relation for the linear growth rate σ as a function of the wavevector q, at the stability boundary for pattern formation ($\beta = 2D(1 + a + 2\sqrt{a})$) with $a = 5$. Middle: the stability boundary dividing the region of parameter space where patterns will form ($\beta > 2D(1 + a + 2\sqrt{a})$) from the region where the homogeneous solution is stable. Right: the wavenumber q_c of the predicted pattern when the system is at the stability boundary. (b) Upper: simulated motor density (solid) and polarity (dashed) for increasing values of β (3, 6, 10; from left to right) with the other parameters: $D = 0.1$, $a = 5$, $\omega = 1$ and $\lambda = 10$. (We use $\lambda = 10$ here and in other simulations because many polymer–motor bundles in the cell are on the order of 10 μm long, which is about ten times the characteristic length for these systems. However, the simulated results are not highly sensitive to the choice of λ.) Here, we are in the regime $\beta > 2D(1 + a + 2\sqrt{a})$, such that pattern formation is expected. Lower: schematics of the sarcomeric pattern (relatively low β) and the graded-polarity pattern (high β).

motors is small, and drift, attachment, detachment, nucleation and disassembly determine the pattern formation.

5. Stability and emergence of patterns in the homogeneous polymer–motor bundle

Equations (6) for the 1-motor system have the constant stationary solution, $p_r = p_l = m = 1$, on the infinite 1D domain (a similar solution exists on a long finite domain with biologically relevant no flux or periodic boundary conditions). This solution describes homogeneous distributions of polymers and motors in the bipolar bundle with polarity equal to zero. To investigate the stability of this state, we turned to the standard procedure of linear stability analysis [40]. We looked for the solutions in the form, $p_r = 1 + \tilde{p}_r$, $p_l = 1 + \tilde{p}_l$, $m = 1 + \tilde{m}$, linearized the equations with respect to $\tilde{p}_r$, $\tilde{p}_l$, $\tilde{m}$, substituted the solutions in the form $\tilde{p}_r, \tilde{p}_l, \tilde{m} \sim \exp[\sigma t]\exp[iqx]$ and obtained the dispersion relations for the linear growth rate σ as a function of the wavevector q. Two branches of this function describe unconditionally stable perturbations, while the third branch gives the potential instability:

$$\sigma = \tfrac{1}{2}\left[-((D+\omega D)q^2 + a + 1) + \left\{((D+\omega D)q^2 + a + 1)^2 - 4\left((Dq^2+1)(\omega D q^2 + a) - \frac{\beta q^2}{2}\right)\right\}^{1/2}\right].$$

Figure 2(a) summarizes findings of the linear stability analysis. Finding maximum of σ with respect to q gives (at $\omega = 1$) a very simple instability criterion: $\beta > 2D(1 + a + 2\sqrt{a})$. In dimensional form:

$$\tilde{V}_0 V_m > 2D_p(\gamma + K_{off} + 2\sqrt{\gamma K_{off}}). \quad (8)$$

Thus, if the product of characteristic motor and polymer speeds is greater than the product of the effective diffusion coefficient and a combination of polymer disassembly and motor detachment rates, the homogeneous un-polarized steady state breaks into a pattern. The instability criterion is especially simple if the motors detach much faster than polymers disassemble: $\tilde{V}_0 V_m > 2D_p K_{off}$. On the other hand, if the motors rarely detach, the instability criterion is $\tilde{V}_0 V_m > 2D_p\gamma$. The known parameters for many motor–polymer systems give $\beta \sim 1$, while $2D(1 + a + 2\sqrt{a}) \sim 2$, so many bundles in the cell are predicted to be homogeneous and un-polarized. However, greater stability of actin filaments and slower detachment of myosin clusters can easily create patterns in the actin–myosin bundles.

When the stability is broken, a periodic pattern should evolve characterized by the wavevector that maximizes $\sigma(q)$: $q_c = \sqrt{\frac{1}{2}[\frac{\beta}{2D^2} - \frac{(a+1)}{D}]}$. Close to the bifurcation point, $q_c \approx (\frac{a}{D^2})^{1/4}$, which indicates that the characteristic

spatial period of the evolving pattern is $l \approx 2\pi(\frac{D_p^2}{K_{off}\gamma})^{1/4} \approx 2\pi(\frac{D_p^3}{\tilde{V}_0 V_m \gamma})^{1/4}$. Substituting characteristic parameter values reveals that the period is a few microns, or a few polymer lengths long. Another important conclusion is that, because of the exponent 1/4 and characteristic parameter ranges, the period of the pattern is very robust and not sensitive to exact parameter values.

We solved equations (6) using Virtual Cell software [41]; our simulations can be reproduced using a public MathModel called 'Cytoskeletal bundle_1-motor' ('Cytoskeletal bundle_2-motor', for the extended model described in section 6) under the username 'ecraig' at the Virtual Cell database (http://vcell.org). Figure 2(b) shows that two general types of patterns evolve. If filament sliding is fast and motor gliding is slow (relatively large β), then the majority of motors gather at the center, and the polarity is perfectly sorted out: filaments in each half of the bundle are oriented with their plus-ends toward the center. On the other hand, if filament sliding is slow and motor gliding is fast (small β), then a periodic pattern evolves resembling sarcomere-like organization of muscle. The period of this pattern is insensitive to values of parameter a. For intermediate values of β, a complex pattern forms: regions of uniform polarity evolve at the edges, while the sarcomeric organization persists at the center. As the polymer speed grows (increasing β), the uniform polarity regions widen, while the number of 'sarcomeres' at the center decrease, until just one motor aggregate at the center is left. If the whole bundle becomes longer, the length of the uniform polarity regions at the edges does not change, rather more 'sarcomeres' appear at the center.

6. Pattern formation by two opposite motors

The case of two opposite motors (2-motor system) can be modeled easily with the following changes in equations (6). The equations for the polymer dynamics become:

$$\partial_t p_{r,l} = \omega D \partial_x^2 p_{r,l} \pm \beta \partial_x \left(\frac{p_r p_l (m_k - m_d)}{p_r + p_l} \right) - p_{r,l} + 1 \quad (9)$$

where m_k and m_d stand for kinesin and dynein concentrations, respectively, assuming that kinesin and dynein actions are linearly additive. Instead of the single equation for the motors, two equations for kinesin and dynein concentrations, respectively, must be considered:

$$\partial_t m_k = D\partial_x^2 m_k - \partial_x \left(\frac{p_l - p_r}{p_r + p_l} m_k \right) + a\,(0.5 + \chi - m_k)\,,$$
$$\partial_t m_d = D\partial_x^2 m_d + \alpha \partial_x \left(\frac{p_l - p_r}{p_r + p_l} m_d \right) + a_d\,(0.5 - \chi - m_d)\,. \quad (10)$$

The new dimensionless parameter a_d describes dynein attachment–detachment kinetics, and the parameter α shows how much faster/slower dynein glides compared to kinesin-5. For simplicity, we assume that the diffusion coefficients of both motors are the same. We calibrate the model so that the total strength of the motors (proportional to the sum of their average concentrations) is the same as that of a single motor in the model above. In the single motor model, the motor average concentration was equal to one; in the two motor model, the sum of the average concentrations is also $(0.5 + \chi + 0.5 - \chi) = 1$. Parameter χ quantifies the relative strength of the motors.

We repeated the linear stability analysis for the two motor model. The new instability criterion has the form:

$$\beta > \frac{4D\left(1 + a + 2\sqrt{a}\right)}{1 + \alpha + \chi\,(1 - \alpha)}, \quad (11)$$

which indicates that if the two motors are of equal strength ($\chi = 0$) and speed ($\alpha = 1$), the stability conditions for the polymer–motor bundle are the same as in the case of the single motor. If the second motor is faster ($\alpha > 1$) or stronger ($\chi > 0$), the instability criterion is lowered such that patterns will arise for smaller values of β than in the case of one motor.

Numerical solutions shown in figure 3 illustrate the characteristic periodic pattern that evolves in this system if the polymer and motors' speeds are fast enough. In this pattern, regions of parallel polymers are interspersed with motor aggregates, and two motor types alternate: dynein aggregates near the minus-ends, and kinesin near the plus-ends. This pattern is very robust—it evolves in a vast range of the parameter space. The period of the pattern is not very sensitive to the ratio β of filament sliding to motor gliding speeds, unlike in the one motor case (figure 3(a)). The period is also insensitive to motor kinetics (parameters a, a_d, α). As the effective diffusion decreases, the pattern's period becomes smaller.

The graded-polarity pattern and the mixed pattern (sarcomeric in the middle, and uniform polarity at the edges) appearing in the single motor case (figure 2(b)) do not emerge for two motors of comparable strengths. However, if one of the motors (dynein, see discussion below) is weaker, and also the polymer sliding is faster than the motors' gliding, then the spindle-like (graded-polarity) pattern evolves (figure 3(b)): the weaker motor aggregates to the edges, the stronger one aggregates to the middle, and microtubules orient with their plus-ends into the center.

7. Influence of autocatalytic polymer nucleation and of long polymers

As discussed above, we find that the periodic sarcomeric pattern is very robust for both the 1-motor and 2-motor systems considered. Here, we discuss several possible mechanisms that could increase the level of robustness of the spindle-like pattern. We find that if we make the rate of motor attachment proportional to the polymer density, the system behavior does not change. Another potentially important factor in the spindle is that short nascent microtubules can form at the sides of the pre-existing polymers [42]. This so-called autocatalytic nucleation was shown to be a very important part of maintaining proper spindle architecture [43]. When we add polymer-induced nucleation to the equations describing polymer dynamics, so that the respective reaction

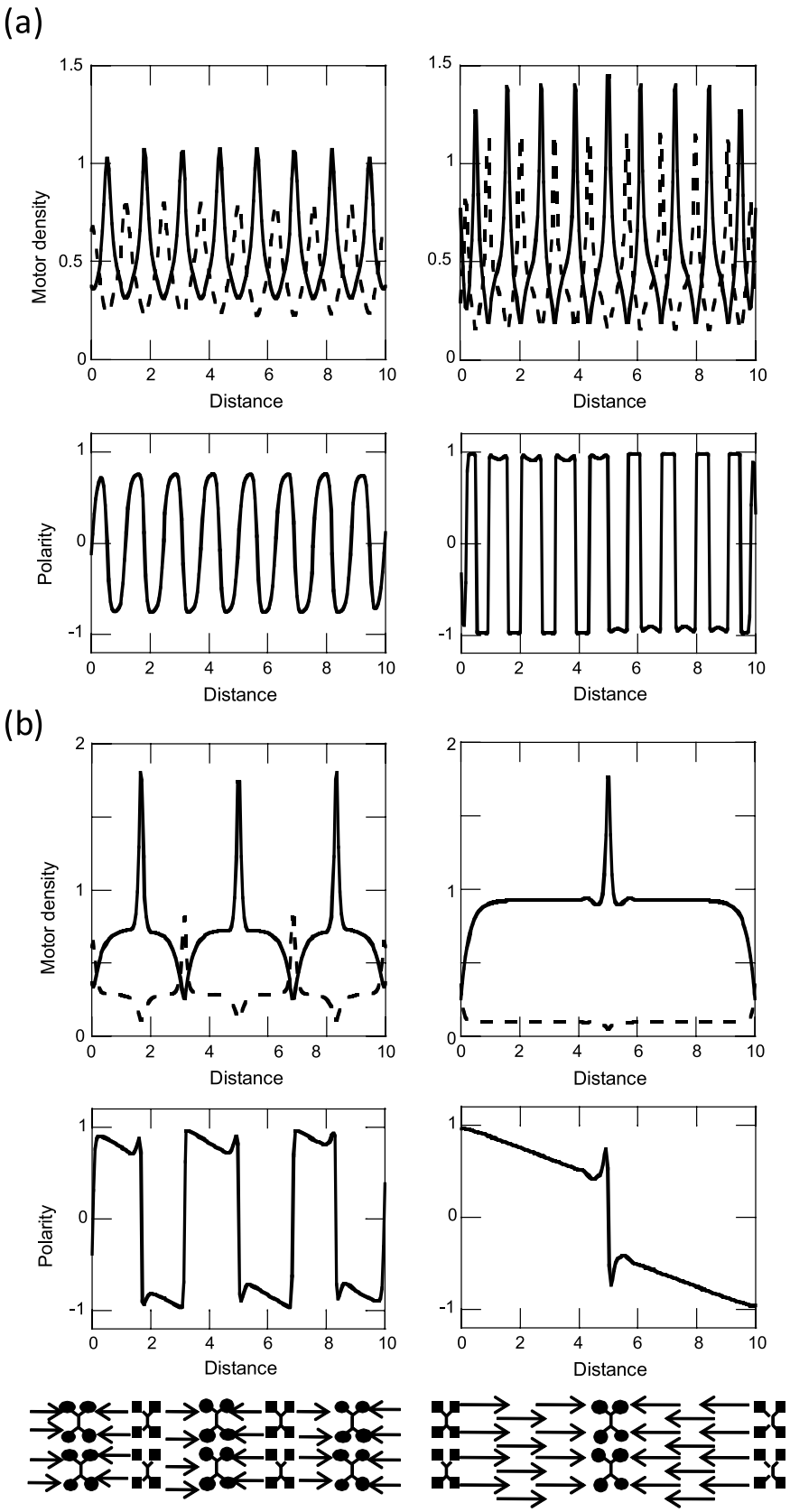

Figure 3. Results for polymer–motor bundles in the 2-motor system. Unless otherwise noted: $D = 0.1$, $\omega = 1$, $a = a_d = 5$ and $\alpha = 1$. (a) Simulations for opposite motors with similar strength ($\chi = 0.05$). Motor density (upper; solid for plus-end motor, dashed for minus-end motor) and polarity (lower) are shown for parameters $\beta = 3$ (left) and $\beta = 10$ (right). (b) Same as (a), with $\beta = 10$, but minus-end motor significantly weaker than plus-end motor ($\chi = 0.2$, 0.4; from left to right), demonstrating recovery of the graded-polarity (spindle-like) pattern when the minus-end motor is weak enough. Lower: schematics of the sarcomeric and graded-polarity patterns, roughly corresponding to the simulations above. Plus-end motors are shown with round motor domains, and minus-end motors with square domains.

terms become $(1 + g(p_r + p_l)^{\varphi} - p_{r,l})$, where g and $\varphi < 1$ are model parameters, the patterns do not change. However, such terms describe autocatalytic nucleation of arbitrary orientation. Not much is known about autocatalytic nucleation of microtubules, but autocatalytic Arp2/3-mediated branching of actin filaments is orientation-specific—daughter filaments grow in the same direction as mother filaments—and it is possible that autocatalytic nucleation of microtubules is characterized by the same feature. To test the consequences of such an assumption, we make the reaction terms look like $(1 + g p_{r,l}^{\varphi} - p_{r,l})$. The results shown in figure 4(a) illustrate that, indeed, such orientation-specific autocatalytic nucleation of microtubules leads to more spindle-like patterns.

The second important factor is that longer microtubules coexist with the short ones in the *in vitro* and meiotic spindles [15, 31]. Including dynamic long microtubules into the model would significantly complicate the mathematics (we intend to work on this in the future), but we can easily add static long microtubules (figure 4(b)) growing from the edges of the bundle (spindle poles) with their plus-ends toward the center (spindle equator), which is the case for *in vivo* mitotic spindles. In the equations, these additional static microtubule densities are added to the dynamic densities $p_{r,l}$, providing additional tracks for the motors and biasing kinesin-5 to the center and dynein to the edges. In the simulations, all added long microtubules were of similar lengths, but we also explored exponential and a couple of other length distributions, and the results were not sensitive to exact functional form of the distributions. As expected, the addition of long microtubules perturbs the sarcomeric pattern and makes it more spindle-like (figure 4(b)).

8. Discussion

The first of the interesting findings from our model is a very simple criterion for the absence of polarity sorting and motor aggregation: the product of the effective polymer diffusion coefficient and polymer disassembly/motor detachment rate (whatever is faster) has to be greater than the product of characteristic motor and polymer speeds. If this inequality is not valid, then patterns emerge. Estimates using data from the literature suggest that characteristic rates in the cell are such that the cytoskeletal bundles are very close to the bifurcation: with a few-fold shift, the cell can easily switch from a 'no pattern' to a 'pattern' state if needed. When the stability is broken, the most ubiquitous, in terms of the largeness of respective domain in the parameter space, is the periodic sarcomere-like pattern, in which periodic regions of alternating polarity (with co-aligned filaments within each region) are interspersed by motor aggregates. Motor aggregates of the same type are spaced a period apart, while two opposite motors create alternating aggregates half a period apart. These patterns evolve if motor gliding is fast.

These results applied to actin–myosin bundles mean that the stability of individual actin filaments is the main condition for evolution of striated stress fibers. Perhaps, this is the reason why large actin arcs and bundles in the rapidly motile cell's appendages, where the actin turnover is generally fast, do not have the stress fibers' structure [8, 33]. A certain degree of global graded actin polarity in such bundles reported in [8, 33] implies, according to our analysis, that myosin cluster gliding is slow, while actin filament sliding is fast in these bundles. This is a prediction to be tested in the future. Similarly, further research will show if complex patterns of actin filaments and unconventional myosin [44], as well as the observed peculiar behavior of the contractile ring consisting of two parallel sub-bundles in the beginning, and of intermingling short filaments in the end [45], have anything to do with the patterns predicted by the model.

Note that our model does not suggest the only, or even the principal, mechanism of assembly of the sarcomeric structure in actin stress fibers [32]. Indeed, the half-period of the predicted periodic structure in our model is a few filament lengths long, while in the classical stress fibers individual filaments seem to span the whole half-period. More importantly, actin binding proteins that are absent in our model clearly play a crucial role in the stress fiber dynamics [32]. Finally, our model does not predict contractile force generation (total flux of actin filaments is zero and the net actin density is constant in the model), while the stress fibers can contract. Nevertheless, it is possible that the periodic pattern instability our model predicts is an integral part of the stress fiber formation, and that the actin binding proteins 'solidify' the emerging pattern.

Applied to *in vitro* and meiotic spindles, the model predicts that if microtubules slide faster than kinesin-5 motors glide, then the global polarity sorting of the microtubules into the characteristic spindle-like configuration would evolve. However, the published data indicate that the kinesin motors are actually faster than the microtubules. Presence of an oppositely directed motor of comparable strength, in fact, additionally destabilizes the graded-polarity bundle. However, the model makes the following important prediction: if the minus-end motor is weaker than kinesin-5, then the spindle-like pattern is restored in the case of fast filament sliding. Interestingly, dynein motors generate force ∼1–1.5 pN [39], weaker than the force (∼5 pN) exerted by kinesin-5 [46]. (There is no data though on relative numbers of these motors in the spindle.) In addition, the model predicts that if nascent microtubules nucleate from the sides of existent ones in the same direction, and/or long microtubules are present in the spindle, then the spindle-like architecture becomes even more stable. Both of these factors are likely at play in *in vitro* and meiotic spindles [15, 42].

Further investigation is needed to see how our model relates to the computational slide-and-cluster model [16] of spindle self-organization, to models of contractile ring dynamics [47, 48] and to the model of self-organization of finite-length polymers [22]. Before such investigation takes place, our model has to include a number of factors omitted in this study for simplicity. Most importantly, a wide variation of the lengths of filaments in the bundles probably has a major impact on the emerging behaviors and patterns [49]. Another factor is that even in the 1D bundles, interactions between the polymers at the core of the bundle and those at the margins have geometric differences, so the description of

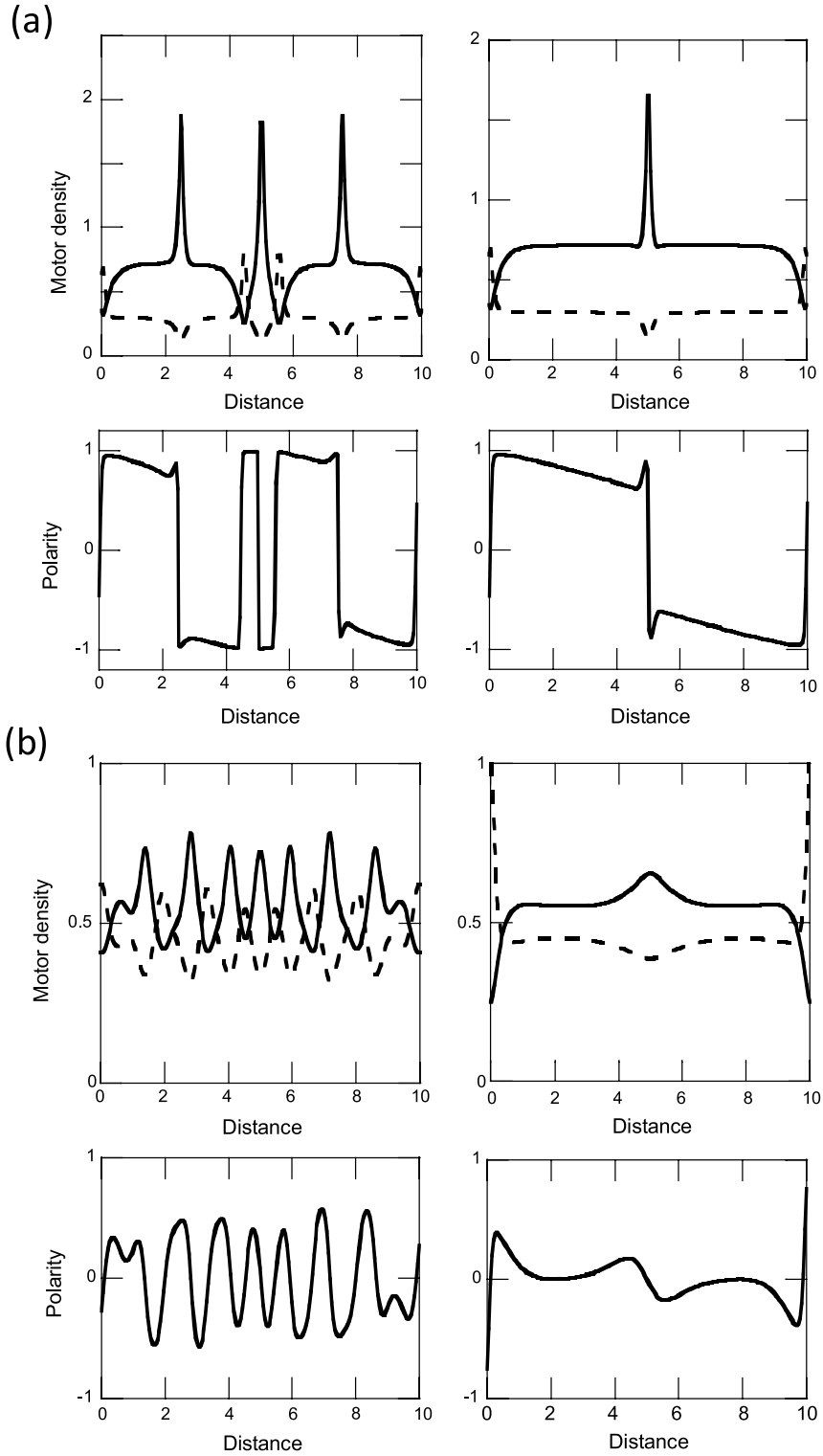

Figure 4. Influence of autocatalytic polymer nucleation and of long polymers on the robustness of the graded-polarity (spindle-like) pattern. Unless otherwise noted: $D = 0.1$, $\omega = 1$, $a = a_d = 5$ and $\alpha = 1$. (a) Motor density (upper; solid line for plus-end motor, dashed line for minus-end motor) and polarity (lower) evolve from the sarcomeric to the graded-polarity pattern as the autocatalytic polymer nucleation increases. Here, we use $g = 2$ (left) and $g = 4$ (right), and for both: $\chi = 0.2$, $\beta = 10$ and $\phi = 0.5$. (b) To include long stationary filaments oriented with their plus-ends toward the center, approximately equal to half the domain length, we model their distribution as step-like functions: $L_r = L_0(\frac{1}{1+e^{-2x}})$ and $L_l = 1 - L_r$, for right oriented and left oriented filaments respectively. Here, we show simulations with long filament density parameter $L_0 = 0.5$. For both: $\beta = 3$ and $\chi = 0.05$. Similarly to (a), motor density (upper; solid line for plus-end motor, dashed line for minus-end motor) and polarity (lower) evolve from the sarcomeric to the graded-polarity pattern as the density of the stationary long filaments increases.

the polymers with continuous density is an approximation to be researched further. Finally, it is unclear what quantitative errors are introduced by continuous approximations of this study and models [20–22] compared to the agent-based simulations [23–25], and how important are the nonlocal [22] effects for the self-organizing patterns. The only consistent way to answer these questions is to study a single model system using the whole spectrum of mathematical and computational approaches.

Acknowledgments

We thank M Rao and K Gowrishankar for fruitful discussions. This work was supported by NIH grant NIGMS GM-068952 and by NSF grant DMS-0315782 to AM.

References

[1] Alberti C 2009 *Eur. Rev. Med. Pharmacol. Sci.* **13** 13–21
[2] Kueh H Y and Mitchison T J 2009 *Science* **325** 960
[3] Civelekoglu-Scholey G and Scholey J M 2010 *Cell. Mol. Life Sci.* **67** 2231
[4] Mitchison T J 1992 *Phil. Trans. R. Soc.* B **336** 99
[5] Discher D E, Janmey P and Wang Y 2005 *Science* **310** 1139
[6] Kumar S, Maxwell I Z, Heisterkamp A, Polte T R, Lele T P, Salanga M, Mazur E and Ingber D E 2006 *Biophys. J.* **90** 3762
[7] Pollard T D 2010 *Curr. Opin. Cell Biol.* **22** 50–6
[8] Svitkina T M, Verkhovsky A B, McQuade K M and Borisy G G 1997 *J. Cell Biol.* **139** 397
[9] Marshall W F 2004 *Annu. Rev. Cell Dev. Biol.* **20** 677
[10] Scholey J M, Brust-Mascher I and Mogilner A 2003 *Nature* **422** 746
[11] Kapitein L C, Peterman E J, Kwok B H, Kim J H, Kapoor T M and Schmidt C F 2005 *Nature* **435** 114
[12] Brust-Mascher I, Civelekoglu-Scholey G, Kwon M, Mogilner A and Scholey J M 2004 *Proc. Natl Acad. Sci. USA* **101** 15938
[13] McDonald K L, O'Toole E T, Mastronarde D N and McIntosh J R 1992 *J. Cell Biol.* **118** 369
[14] Heald R, Tournebize R, Blank T, Sandaltzopoulos R, Becker P, Hyman A and Karsenti E 1996 *Nature* **382** 420
[15] Yang G, Houghtaling B R, Gaetz J, Liu J Z, Danuzer G and Kapoor T M 2007 *Nat. Cell Biol.* **9** 1233
[16] Burbank K S, Mitchison T J and Fisher D S 2007 *Curr. Biol.* **17** 1373
[17] Walczak C E and Heald R 2008 *Int. Rev. Cytol.* **265** 111
[18] Brunet S, Polanski Z, Verlhac M H, Kubiak J Z and Maro B 1998 *Curr. Biol.* **8** 1231
[19] Khodjakov A, Cole R W, Oakley B R and Rieder C L 2000 *Curr. Biol.* **10** 59–67
[20] Kruse K, Zumdieck A and Jülicher F 2003 *Europhys. Lett.* **64** 716
[21] Lee H Y and Kardar M 2001 *Phys. Rev.* E **64** 056113
[22] Kruse K and Jülicher F 2000 *Phys. Rev. Lett.* **85** 1778
[23] Nédélec F 2002 *J. Cell Biol.* **158** 1005
[24] Schaffner S C and José J V 2006 *Proc. Natl Acad. Sci. USA* **103** 11166
[25] Zemel A and Mogilner A 2009 *Phys. Chem. Chem. Phys.* **11** 4821
[26] Shlomovitz R and Gov N S 2007 *Phys. Rev. Lett.* **98** 168103
[27] Bormuth V, Varga V, Howard J and Schäffer E 2009 *Science* **325** 870
[28] Maly I V 2002 *Bull. Math. Biol.* **64** 213
[29] Andrianantoandro E, Blanchoin L, Sept D, McCammon J A and Pollard T D 2001 *J. Mol. Biol.* **312** 721
[30] Andrianantoandro E and Pollard T D 2006 *Mol. Cell* **24** 13–23
[31] Needleman D J, Groen A, Ohi R, Maresca T, Mirny L and Mitchison T 2010 *Mol. Biol. Cell* **21** 323
[32] Naumanen P, Lappalainen P and Hotulainen P J 2008 *J. Microsc.* **231** 446
[33] Mseka T, Coughlin M and Cramer L P 2009 *Cell Motil. Cytoskeleton* **66** 743
[34] Cheerambathur D K, Civelekoglu-Scholey G, Brust-Mascher I, Sommi P, Mogilner A and Scholey J M 2007 *J. Cell Biol.* **177** 995
[35] Cheerambathur D K, Brust-Mascher I, Civelekoglu-Scholey G and Scholey J M 2008 *J. Cell Biol.* **182** 429
[36] Schaub S, Bohnet S, Laurent V M, Meister J J and Verkhovsky A B 2007 *Mol. Biol. Cell* **18** 3723
[37] Miyamoto D T, Perlman Z E, Burbank K S, Groen A C and Mitchison T J 2004 *J. Cell Biol.* **167** 813
[38] Wang H, Brust-Mascher I, Cheerambathur D and Scholey J M 2010 *Cytoskeleton* **67** 715
[39] McKenney R J, Vershinin M, Kunwar A, Vallee R B and Gross S P 2010 *Cell* **141** 304
[40] Edelstein-Keshet L 2005 *Mathematical Models in Biology* (Philadelphia, PA: SIAM)
[41] Slepchenko B M and Loew L M 2010 *Int. Rev. Cell Mol. Biol.* **283** 1
[42] Goshima G and Kimura A 2010 *Curr. Opin. Cell Biol.* **22** 44–9
[43] Clausen T and Ribbeck K 2007 *PLoS One* **2** e244
[44] Brawley C M and Rock R S 2009 *Proc. Natl Acad. Sci. USA* **106** 9685
[45] Kamasaki T, Osumi M and Mabuchi I 2007 *J. Cell Biol.* **178** 765
[46] Valentine M T, Fordyce P M, Krzysiak T C, Gilbert S P and Block S M 2006 *Nat. Cell Biol.* **8** 470
[47] Carlsson A E 2006 *Phys. Rev.* E **74** 051912
[48] Zumdieck A, Kruse K, Bringmann H, Hyman A A and Jülicher F 2007 *Plos One* **2** e696
[49] Baas P W, Vidya Nadar C and Myers K A 2006 *Traffic* **7** 490